

Highlights

DMC-Net: Lightweight Dynamic Multi-Scale and Multi-Resolution Convolution Network for Pancreas Segmentation in CT Images

Jin Yang, Daniel S. Marcus, Aristeidis Sotiras

- 2D and 3D Dynamic Multi-scale and Multi-resolution Convolution network for pancreas and pancreatic tumor segmentation
- Dynamic Multi-Scale Convolution (DMSC) and Dynamic Multi-Resolution Convolution (DMRC) to dynamically capture features at varying scales and adaptively utilize global contextual information
- The lightweight design for DMSC and DMRC to reduce computational complexity.
- The proposed method achieves superior segmentation performance over state-of-the-art methods on pancreas segmentation in CT images.

DMC-Net: Lightweight Dynamic Multi-Scale and Multi-Resolution Convolution Network for Pancreas Segmentation in CT Images

Jin Yang^a, Daniel S. Marcus^a and Aristeidis Sotiras^{a,b,**}

^aMallinckrodt Institute of Radiology, Washington University School of Medicine in St. Louis, St. Louis, 63110, MO, USA

^bInstitute for Informatics, Data Science and Biostatistics, Washington University School of Medicine in St. Louis, St. Louis, 63110, MO, USA

ARTICLE INFO

Keywords:

Dynamic Convolution
Multi-scale Convolution
Multi-resolution Convolution
Lightweight Network
Pancreas Segmentation

ABSTRACT

Background and Objective: Convolutional neural networks (CNNs) have shown great effectiveness in medical image segmentation. However, they may be limited in modeling large inter-subject variations in organ shapes and sizes and exploiting global long-range contextual information. This is because CNNs typically employ convolutions with fixed-sized local receptive fields and lack the mechanisms to utilize global information.

Methods: To address these limitations, we developed Dynamic Multi-Resolution Convolution (DMRC) and Dynamic Multi-Scale Convolution (DMSC) modules. Both modules enhance the representation capabilities of single convolutions to capture varying scaled features and global contextual information. This is achieved in the DMRC module by employing a convolutional filter on images with different resolutions and subsequently utilizing dynamic mechanisms to model global inter-dependencies between features. In contrast, the DMSC module extracts features at different scales by employing convolutions with different kernel sizes and utilizing dynamic mechanisms to extract global contextual information. The utilization of convolutions with different kernel sizes in the DMSC module may increase computational complexity. To lessen this burden, we propose to use a lightweight design for convolution layers with a large kernel size. Thus, DMSC and DMRC modules are designed as lightweight drop-in replacements for single convolutions, and they can be easily integrated into general CNN architectures for end-to-end training. The segmentation network was proposed by incorporating our DMSC and DMRC modules into a standard U-Net architecture, termed Dynamic Multi-scale and Multi-resolution Convolution network (DMC-Net).

Results: To evaluate their effectiveness, we conducted experiments on pancreas segmentation from abdominal computed tomography (CT) images with the DMC-Net. The results demonstrate that our proposed DMSC and DMRC can enhance the representation capabilities of single convolutions and improve segmentation accuracy. Furthermore, their lightweight design led to lower computational complexity while maintaining or improving segmentation performance.

Conclusions: The DMC-Net outperformed the state-of-the-art methods on pancreas segmentation in CT images.


1. Introduction

Medical image segmentation is a critical task in clinical practice as it enables clinicians to locate target organs, quantify their anatomy, understand their morphology, and detect anatomical changes, thereby enabling accurate diagnosis and treatment planning. However, manual pixel-level labeling is time-consuming and error-prone. Therefore, automated segmentation tools are in high demand. Deep learning has revolutionized the field of image segmentation, and deep learning-based methods have been successful at troubleshooting semantic segmentation and instance segmentation problems Chen et al. (2016); Noh et al. (2015); Badrinarayanan et al. (2017); Hariharan et al. (2014); Isensee et al. (2021). In particular, convolutional neural networks (CNNs) have emerged as a robust, effective, and popular tool in automatic medical image segmentation,

due to their high representation power, fast inference, and weight-sharing properties. Ronneberger et al. (2015); Zhou et al. (2018); Çiçek et al. (2016). Indeed, CNNs have become the de facto standard for object segmentation in various medical imaging modalities, e.g., magnetic resonance (MR) Milletari et al. (2016), computed tomography (CT) Ibragimov and Xing (2017); Yang et al. (2023), positron emission tomography (PET) Zhao et al. (2018), and X-ray Narin et al. (2021).

The pancreas is a crucial organ for digestion and glucose metabolism, and pancreatic cancer is the fourth leading cause of cancer-related death due to its inferior prognosis McGuigan et al. (2018). Thus, accurate segmentation of pancreas and pancreatic masses is essential for the diagnosis and treatment of pancreas diseases. However, pancreas segmentation from abdominal CT images is challenging due to the substantial inter-patient variations in shape and size. Additionally, the pancreas only occupies a tiny part of the image. To solve this problem, several CNN-based methods have been proposed in recent years due to their

**Corresponding author

 yang.jin@wustl.edu (J. Yang); aristeidis.sotiras@wustl.edu (A. Sotiras)

ORCID(s):

superior segmentation capabilities Kumar et al. (2019). However, existing applications for pancreas segmentation rely heavily on multi-stage cascaded CNN frameworks Roth et al. (2017); Zhou et al. (2017); Cai et al. (2017); Zhao et al. (2019a); Zhang et al. (2021a). These frameworks typically employ CNNs (or other methods) in the first stage to make initial predictions and to identify a region of interest (ROI). In the second stage, CNNs are applied to make final dense predictions on that particular ROI, thus improving the overall segmentation accuracy of the single model. However, cascaded approaches lead to excessive and redundant use of computational resources and model parameters, as all models within the cascaded frameworks repeatedly extract similar low-level features. To enhance segmentation efficiency, one-stage CNN models have been proposed Schlemper et al. (2019); Zhang et al. (2021c). However, these models employ convolutions with fixed-sized local receptive fields, thus limiting their ability to segment organs with large inter-patient variations in shape and size and to utilize global contextual information outside receptive fields.

Several methodologies have been put forward to enhance convolutions with capabilities to capture features with varying shapes and scales. Feature pyramid methods were proposed to combine feature maps at different scales from different layers in a pyramidal hierarchic structure, enhancing the ability of the networks to make predictions on varying-scaled features Lin et al. (2017); Seferbekov et al. (2018); Zhao et al. (2019b). Additionally, multi-branch segmentation networks employed multiple segmentation paths to encode information at different scales Wang et al. (2015); Aslani et al. (2019); Chen et al. (2022a). However, these prior works focus on changing the macro-architecture of neural networks to use varying scaled features and may not be readily integrated into general CNN structures, which limits their applicability. Moreover, the implementation of these methods leads to a significant increase in the model size and computational complexity of the network, hindering their wide use for medical image segmentation.

Other methods employ convolutional layers with both small and large kernel sizes to extract multi-scale features Yang et al. (2023); He et al. (2019). However, employing large convolutional kernels may lead to an increase in computational complexity. Previously, atrous convolutions with a large kernel size were applied since they can provide a large receptive field and alleviate computational burdens Chen et al. (2017); Hu et al. (2020). However, this is achieved by reducing the number of grid samples within receptive fields, thus reducing representation capabilities and lowering the accuracy of dense prediction. An alternative way is highly demanded to reduce computational complexity while maintaining or improving representation capabilities.

Additionally, another limitation of CNNs lies in the inability of convolution layers to adaptively calibrate features using

global contextual information. Some existing attention-based methods can tackle this problem Hu et al. (2018); Woo et al. (2018); Fu et al. (2019); Zhong et al. (2020). These methods were designed to model channel or spatial inter-dependencies among features, and then use the global information to selectively emphasize informative features and suppress less useful ones. However, these are designed as independent modules to improve the whole network rather than directly improving convolution layers, thus limiting their applicability and interpretability.

In this paper, we aim to address these limitations by developing efficient solutions, specifically Dynamic Multi-Scale Convolution (DMSC) and Dynamic Multi-Resolution Convolution (DMRC). Both DMSC and DMRC modules are designed to enhance the capabilities of convolution layers to capture varying scaled features and utilize global contextual information to recalibrate local features. In the DMSC module, features at various scales are extracted by convolutions with different kernel sizes. Employing multiple convolutional layers increases the width of the network and enlarges the receptive field. Inspired by the recent works on large kernel-based CNNs Ding et al. (2022); Guo et al. (2022); Lee et al. (2022); Yang et al. (2024), we propose to use depth-wise convolutions to reduce computational complexity. Subsequently, channel-wise dynamic mechanisms are used to model inter-dependencies between channel features extracted by two convolutions, thus calibrating these features via global information. In contrast, in the DMRC module, a convolution layer is employed on images with different resolutions to extract features at various scales, including pixel-wise and region-wise ones. Subsequently, the same dynamic mechanisms are applied to capture channel-wise global information. We designed our DMSC and DMRC as drop-in replacements of convolution layers, allowing for easy integration into existing CNN architectures without the need for changing their macro-architectures. CNNs equipped with DMSC or DMRC may be trained end-to-end for segmentation in the same manner as the original ones.

To evaluate the effectiveness of our DMSC and DMRC in segmentation tasks, we integrated them into a general CNN architecture to generate our segmentation network, namely Dynamic Multi-scale and Multi-resolution Convolution Network (DMC-Net). Specifically, a U-Net is used as the backbone Ronneberger et al. (2015), and DMSC and DMRC are incorporated into it by replacing standard convolutions. Since U-Net employs standard convolution layers to extract fixed-scaled local features for segmentation without the utilization of global contextual information, it is straightforward to evaluate the benefits of our modules. To demonstrate these benefits, we evaluated our implementation on two commonly used abdominal CT pancreas segmentation benchmarks, namely the NIH The Cancer Imaging Archive Pancreas CT (TCIA-Pancreas) Holger et al.

(2016) for healthy pancreas segmentation and the Medical Segmentation Decathlon Pancreas challenge (MSD-Pancreas) Antonelli et al. (2022) for the segmentation of the pancreas and pancreatic masses. Our results indicate that our segmentation network achieved superior segmentation performance compared to state-of-the-art methods. Importantly, DMC-Net using DMSC and DMRC modules achieved significant improvements over the standard U-Net baseline that uses standard convolutional layers. Lastly, the lightweight design of the convolutional layers led to lower computational complexity without compromising segmentation performance.

Our contributions can be summarized as follows.

- We developed two novel modules, Dynamic Multi-Scale Convolution (DMSC) and Dynamic Multi-Resolution Convolution (DMRC), to enhance the capabilities of convolutional layers. These modules dynamically capture features at varying scales and adaptively utilize global contextual information to recalibrate features. Both of them are designed as 2D and 3D drop-in blocks, allowing for easy integration into existing CNN architectures by replacing convolutional layers without the need for changing their macro-architectures. CNNs equipped with DMSC or DMRC can be trained end-to-end for segmentation.
- We proposed lightweight designs for the DMRC and DMSC modules. These designs can reduce the computational complexity of segmentation models while maintaining or improving their representation capabilities.
- We generated a 2D and 3D Dynamic Multi-scale and Multi-resolution Convolution network (2D-DMC-Net and 3D-DMC-Net) for automatic medical image segmentation by incorporating DMSC and DMRC modules into a standard 2D and 3D U-Net, respectively.
- Our experimental results in pancreas segmentation demonstrate that replacing convolutional layers with DMSC or DMRC in the U-Net architecture improves segmentation accuracy. Additionally, the proposed DMC-Net showed superior performance over state-of-the-art pancreas segmentation methods.

2. Methods

We propose 2D and 3D Dynamic Multi-Scale Convolution (DMSC) and Dynamic Multi-Resolution Convolution (DMRC) modules, and the incorporation of them into 2D and 3D backbones generate 2D and 3D Dynamic Multi-scale and Multi-resolution Convolution networks (2D-DMC-Net and 3D-DMC-Net). To simplify the presentation, we will focus on describing the 2D modules and the 2D network in this section and highlighting any potential differences between the 2D and 3D implementations at the end of the section.

2.1. Network architecture

We propose a Dynamic Multi-Scale and Multi-Resolution Convolution network (DMC-Net) for the automatic pancreas and pancreatic mass segmentation. This model was designed based on integrating DMSC and DMRC modules into a standard U-Net backbone Ronneberger et al. (2015). Specifically, DMRC was placed after DMSC, and we used them to replace convolutional layers at each layer. 2×2 Max-pooling layers and 3×3 transposed convolutional layers were used to downscale and upscale the feature maps. They were also used to increase and decrease the number of feature maps, respectively. At the final layer, a 1×1 convolution was used to generate the segmentation prediction. The proposed 2D-DMC-Net has 6 layers, and the number of feature maps in each layer was 32, 64, 128, 256, 512, and 512, respectively (Figure 1). The proposed 3D-DMC-Net has 5 layers with 32, 64, 128, 256, and 512 feature maps, respectively (Figure 2).

2.2. Dynamic Multi-Resolution Convolution (DMRC)

We propose the Dynamic Multi-Resolution Convolution (DMRC) module to dynamically capture features at various scales. This is achieved by employing convolutions on images with different resolutions and adaptively utilizing global contextual information (2D: Figure 1; 3D: Figure 2). Specifically, three parallel paths are adopted to generate multi-scale features from input feature maps $\mathbf{X} = [\mathbf{x}_1, \mathbf{x}_2, \dots, \mathbf{x}_C] \in \mathbb{R}^{C \times H \times W}$. First, a convolutional layer with a kernel size of 3, denoted as $\mathcal{F}_{conv}(\cdot)$, is applied to extract features $\mathbf{F}_1 \in \mathbb{R}^{C \times H \times W}$ from the input \mathbf{X} with the original resolution:

$$\mathbf{F}_1 = \mathcal{F}_{conv}(\mathbf{X}).$$

The second path employs a convolutional layer to extract features at another scale $\mathbf{F}_2 \in \mathbb{R}^{C \times H \times W}$ by utilizing neighboring contextual information from the input \mathbf{X} . Specifically, this path first utilizes average pooling $\mathcal{F}_{AvgPool}(\cdot)$ operation with 4×4 filter and 4×4 stride to capture and aggregate neighboring contextual information from input feature maps \mathbf{X} , effectively reducing their resolution by 4. Subsequently, a 3×3 convolution, denoted as $\mathcal{F}_{conv}(\cdot)$, is applied to generate features $\mathbf{F}_2 \in \mathbb{R}^{C \times \frac{H}{4} \times \frac{W}{4}}$ from rescaled images. Thus, these features \mathbf{F}_2 are at different scales from features \mathbf{F}_1 . Lastly, nearest neighbor interpolation $\mathcal{F}_{up}(\cdot)$ is used to upsample these features \mathbf{F}_2 to the original input dimension. These operations are summarized in the equation below:

$$\mathbf{F}_2 = \mathcal{F}_{up}(\mathcal{F}_{conv}(\mathcal{F}_{AvgPool}(\mathbf{X}))).$$

However, aggregating neighboring contextual information by average pooling may lead to the loss of pixel-wise information. This limitation is solved by the third path. This path employs a 1×1 convolution layer, denoted as $\mathcal{F}_{conv}^{(1)}(\cdot)$, to extract pixel-wise contextual information $\mathbf{F}_3 \in \mathbb{R}^{C \times H \times W}$:

$$\mathbf{F}_3 = \mathcal{F}_{conv}^{(1)}(\mathbf{X}).$$

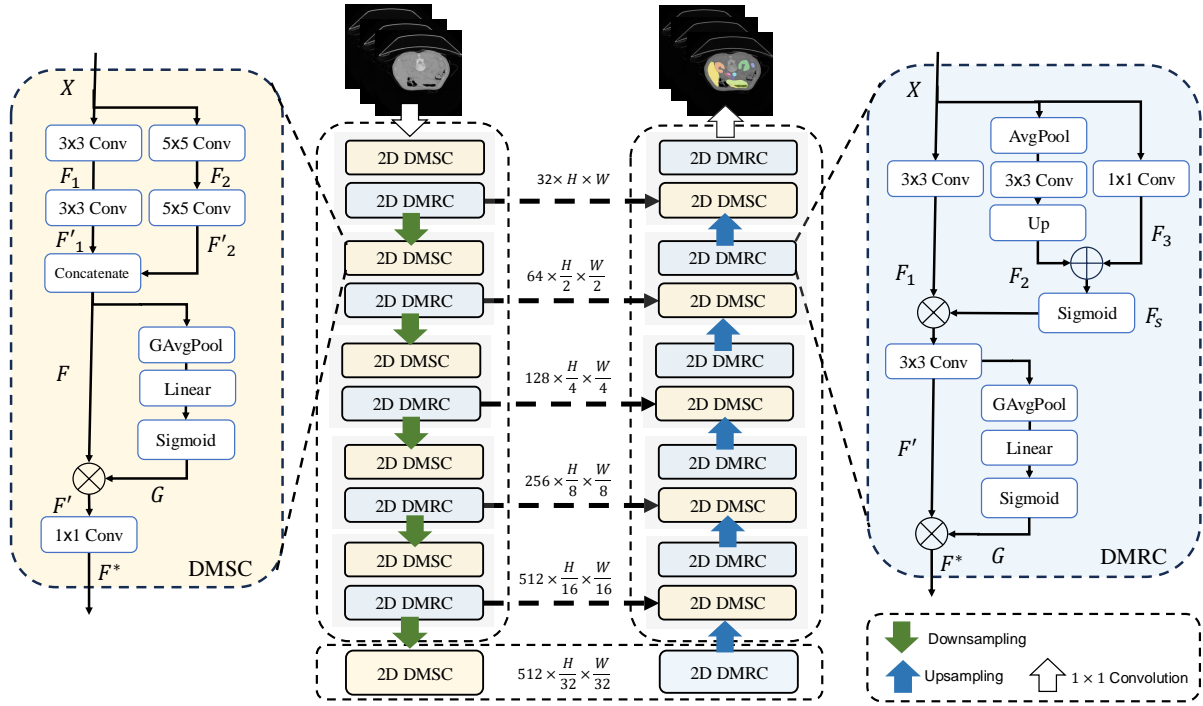


Figure 1: The architecture of 2D DMC-Net. It is designed as a U-shaped network, consisting of a 5-stage encoder, a 5-stage decoder, and a bottleneck. In each stage, the basic block consists of a 2D DMSC module and a 2D DMRC module. A 1×1 convolutional layer is utilized to project input features to 32 channels in the encoder, and another 1×1 convolutional layer is utilized to make pixel-wise predictions in the decoder.

Subsequently, the pixel-wise information F_3 and neighboring region-wise features F_2 are fused to generate the features $F_s \in \mathbb{R}^{C \times H \times W}$:

$$F_s = F_2 \oplus F_3.$$

When generating multi-scale features $F \in \mathbb{R}^{C \times H \times W}$ by fusing features in three paths F_1 and F_s , we utilize a spatial-wise dynamic mechanism. Specifically, a Sigmoid function $\mathcal{F}_{Sig}(\cdot)$ is used to convert features F_s to attention values, which are then utilized to calibrate features F_1 via element-wise multiplication:

$$F = F_1 \otimes \mathcal{F}_{Sig}(F_s).$$

In the subsequent step, another 3×3 convolution layer $\mathcal{F}_{conv}^{(3)}(\cdot)$ is utilized to extract organ-specific spatial features and generate feature maps $F' \in \mathbb{R}^{C \times H \times W}$:

$$F' = \mathcal{F}_{conv}^{(3)}(F).$$

We utilize dynamic mechanisms to capture global information $G \in \mathbb{R}^{C \times 1 \times 1}$ by modeling channel-wise interdependencies among features F' . This is achieved by cascading a global average pooling $\mathcal{F}_{AvgPool}(\cdot)$, a Linear layer $\mathcal{F}_{Conv}^{(1)}(\cdot)$, and a Sigmoid activation $\mathcal{F}_{Sig}(\cdot)$:

$$G = \mathcal{F}_{Sig}(\mathcal{F}_{Conv}^{(1)}(\mathcal{F}_{AvgPool}(F'))).$$

Finally, the output features of the DMRC module $F^* \in \mathbb{R}^{C_{out} \times H \times W}$ are generated by using this global information

G to dynamically calibrate multi-resolution features F' :

$$F^* = F' \otimes G.$$

3D implementation details: There are a few differences between 2D and 3D implementations that we would like to highlight. Let $X = [x_1, x_2, \dots, x_C] \in \mathbb{R}^{C \times D \times H \times W}$ be input feature maps. In the second path, average pooling operations with $1 \times 4 \times 4$ filter and $1 \times 4 \times 4$ stride are applied for X .

2.3. Dynamic Multi-Scale Convolution (DMSC)

We propose the Dynamic Multi-Scale Convolution (DMSC) module to dynamically capture varying-scaled features. This is achieved by employing convolutions with multi-scale kernels and adaptively utilizing global contextual information (2D: Figure 1; 3D: Figure 2). Two parallel paths are adopted to capture features at varying scales from input feature maps $X = [x_1, x_2, \dots, x_C] \in \mathbb{R}^{C \times H \times W}$. Convolutions with different kernel sizes of 3 and 5, denoted as $\mathcal{F}_{conv}^{(3)}(\cdot)$ and $\mathcal{F}_{conv}^{(5)}(\cdot)$, are employed in each path (see Eq. 1 and Eq. 2). Application of convolutions in parallel paths results in their increased width to capture finer-grained features, thus granting DMSC enhanced representation capabilities over the single convolution. Moreover, our design employs receptive fields of various sizes, which helps convolutions extract features at different scales.

$$F_1 = \mathcal{F}_{conv}^{(3)}(X). \quad (1)$$

$$F_2 = \mathcal{F}_{conv}^{(5)}(X). \quad (2)$$

with a kernel size of 5. However, they may result in a lower segmentation performance and significantly increase computational complexity.

Lastly, to enable convolutional layers to extract features from input images with different sizes, we applied average pooling operations with 4×4 filters and 4×4 stride in 2D DMRC modules and with $1 \times 4 \times 4$ filters and $1 \times 4 \times 4$ stride in 3D DMRC modules. This is an optimal lightweight design because it can improve segmentation performance while decreasing computational complexity. In contrast, using average pooling operations with 2×2 filters and 2×2 stride in 2D DMRC modules, and with $1 \times 2 \times 2$ filters and $1 \times 2 \times 2$ in 3D DMRC modules leads to higher computational complexity and potentially lower segmentation accuracy.

3. Experiments and Results

3.1. Datasets

We conducted experiments on two publicly available datasets. The first dataset used was the National Institutes of Health (NIH) repository of normal pancreas CTs, which is made publicly available through The Cancer Imaging Archive (TCIA-Pancreas) Holger et al. (2016). This dataset comprises 80 contrast-enhanced 3D abdominal CT scans obtained from patients who had neither major abdominal pathologies nor pancreatic cancer lesions. The original CT scans have a resolution of 512×512 pixels with varying pixel sizes and slice thickness between 1.5 mm and 2.5 mm . The number of slices ranges from 181 to 466 varying from patient to patient. Manual annotations of the pancreas were conducted slice-by-slice by a medical student and were then verified and refined by an experienced radiologist. These annotations were used as the segmentation ground truth for this dataset.

Additionally, we utilized the public abdominal CT pancreas dataset from the Medical Segmentation Decathlon challenge (MSD-Pancreas; MICCAI 2018) Antonelli et al. (2022), which was acquired at the Memorial Sloan Kettering Cancer Center (New York, NY, USA). This dataset consists of 420 portal-venous phase CT scans of patients undergoing resection of pancreatic masses and is divided into 281 training and 139 testing scans. The raw training CT scans have resolutions of 512×512 pixels with varying pixel sizes and slice thickness. The number of slices in the axial view ranges from 37 to 751. Manual annotations were performed for both pancreatic parenchyma and pancreatic mass (i.e., cyst or tumor), and three semantic classes were provided, namely pancreas, pancreatic mass, and background. In our experiments, we used only the training samples since these were the only ones that were accompanied by annotations.

3.2. Implementation details

The DMC-Net was implemented using PyTorch. We used a combination of cross-entropy loss \mathcal{L}_{CE} and dice loss \mathcal{L}_{Dice} . The loss function \mathcal{L} can be formulated between the

prediction \hat{y} and the target y as:

$$\mathcal{L} = \mathcal{L}_{CE}(\hat{y}, y) + \mathcal{L}_{Dice}(\hat{y}, y).$$

During training, the stochastic gradient descent (SGD) optimizer was used for model optimization. The initial learning rate was set to 0.001 with a Nesterov momentum of 0.99 and it was decayed with a poly learning rate scheduler during training. The number of training epochs was set to 1000 for all training sessions. The batch size was 12 and 2 for 2D and 3D data, respectively. Models were trained and validated on NVIDIA Tesla A100 PCI-E Passive Single GPU each with 40GB of GDDR5 memory. The code will be made available from the lab Github upon acceptance for publication.

Several pre-processing techniques were implemented for images from both two datasets. Firstly, volumetric scans were resampled to a resolution of $0.85 \times 0.85 \times 1.0 \text{ mm}^3$ and $0.8 \times 0.8 \times 2.5 \text{ mm}^3$ in TCIA-Pancreas and MSD-Pancreas datasets, respectively. Subsequently, we normalized intensity values by performing min-max normalization over the whole volume. Finally, data were prepared as 2D patches with size $512 \times 512 \text{ mm}^2$ and 3D patches with size $192 \times 192 \times 96 \text{ mm}^3$ in the TCIA-Pancreas dataset. Additionally, data were prepared as 2D patches with size $512 \times 512 \text{ mm}^2$ and 3D patches with size $192 \times 192 \times 64 \text{ mm}^3$ in the MSD-Pancreas dataset.

Several data augmentation techniques were implemented. Patches were rotated along three axes between $[-30, 30]$ and scaled between $(0.7, 1.4)$ with a probability of 0.2. All patches were mirrored with a probability of 0.5 along all axes. Zero-centered additive Gaussian noise with the variance drawn from $U(0, 0.1)$ was added to each voxel in the sample with a probability of 0.15. Gaussian blur was applied with a probability of 0.2 for each sample by a Gaussian kernel whose width is sampled from $U(0.5, 1.5)$. Brightness and contrast were applied to voxel intensities both with a probability of 0.15.

We employed a 5-fold cross-validation approach to get stable and reliable evaluation results on both two benchmarks. Segmentation performance was evaluated by two metrics: Dice Similarity Coefficient (DSC) and 95% Hausdorff distance (95HD). The architecture complexity was evaluated by two metrics: the number of parameters (Params) and the number of Floating Point Operations (FLOPs). The Wilcoxon signed-rank test was implemented to statistically quantify the differences in segmentation performance.

3.3. Comparison to state-of-the-art frameworks

We compared the proposed model with state-of-the-art (SOTA) models on two datasets. These SOTA methods have been previously applied to segment the pancreas on the TCIA dataset and pancreatic tumors on the MSD dataset.

On the NIH TCIA-Pancreas dataset, we compared 2D-DMC-Net with three 2D state-of-the-art models, namely

Table 1

Performance comparison between our approach and the state-of-the-art methods for pancreas segmentation on the NIH TCIA-Pancreas dataset. Segmentation performance was evaluated by DSC (%). The DSC is reported as mean±std. The best performance for each class of models is highlighted by **bold**.

Models	Methods	Mean DSC	Max DSC	Min DSC
2D	C-RNN	82.4±6.7	90.1	60.0
	RSTN	84.50±4.97	91.02	62.81
	TVMS-Net	85.19±4.73	91.42	68.69
	DMC-Net (ours)	85.64±3.93	90.86	77.20
2.5D	DeepOrgan	71.8±10.7	86.9	25.0
	HNN	81.14±7.30	89.98	44.69
	Fixed-point	82.37±5.68	90.85	62.43
	DSD-ASPP-Net	85.49±4.77	91.64	67.19
	DCNN	84.90	91.02	62.81
	MADC-Net	86.49±1.44	-	-
	RTUNet	86.25±4.52	93.02	72.55
3D	Attention U-Net	81.48±6.23	-	-
	CNN	84.47±4.36	91.54	70.61
	ECTN	85.58±3.98	91.30	72.88
	DMC-Net (ours)	87.97±3.52	91.56	77.64

Table 2

Performance comparison between our approach and state-of-the-art methods for pancreas and pancreatic tumor segmentation on the MSD-Pancreas dataset. Segmentation performance was evaluated by Mean DSC (%). Our experiments were implemented using 5-fold cross-validation following the same partition as nnU-Net [Isensee et al. \(2021\)](#). The best and second performances are highlighted by **bold** and underline.

Models	Methods	Pancreas DSC	Tumor DSC	Average DSC
2D	nnU-Net	77.38	35.01	56.19
	DMC-Net (ours)	79.82	42.07	60.95
3D	V-Net	79.01	35.99	57.50
	V-NAS	79.9	38.78	59.34
	C2FNAS	80.59	52.87	66.73
	nnU-Net	<u>82.14</u>	54.28	<u>68.21</u>
	SAR	73.42	25.19	49.31
	Distill DSM	79.20	37.65	58.43
	DiNTS	81.02	<u>55.35</u>	68.19
	HyperSegNAS	79.98	54.88	67.43
	DMC-Net (ours)	82.92	60.71	71.81

C-RNN [Cai et al. \(2017\)](#), RSTN [Yu et al. \(2018\)](#), TVMS-Net [Chen et al. \(2022b\)](#). Additionally, we compared 3D-DMC-Net with seven 2.5D state-of-the-art models, namely DeepOrgan [Roth et al. \(2015\)](#), HNN [Roth et al. \(2018\)](#), Fixed-points [Zhou et al. \(2017\)](#), DSD-ASPP-Net [Hu et al. \(2020\)](#), DCNN [Zhang et al. \(2021a\)](#), MADC-Net [Li et al. \(2022\)](#), and RTUNet [Qiu et al. \(2023\)](#), and three 3D state-of-the-art models, namely Attention U-Net [Schlemper et al. \(2019\)](#), CNN [Zhang et al. \(2021c\)](#), and ECTN [Zheng and Luo \(2023\)](#). Table 1 presents the comparison results of these methods. When our 2D-DMC-Net is compared with other 2D models, it outperforms these models and achieves the highest Mean DSC value, showing the effectiveness of our proposed model. Additionally, 2D-DMC-Net shows the

lowest standard deviation in Mean DSC and the smallest gap between Max DSC and Min DSC, which demonstrates the robustness of our model in pancreas segmentation. Both 2.5D models and 3D models account for the 3D nature of volume data, so we compare our 3D DMC-Net with other 2.5D and 3D models. Our 3D-DMC-Net demonstrates a superior segmentation performance than other methods. Specifically, it shows the highest Mean DSC in pancreas segmentation. Moreover, it achieves the highest robustness than other methods due to the smallest standard deviation in Mean DSC and the smallest gap between Max DSC and Min DSC.

Table 3

The results of the ablation study on TCIA-Pancreas and MSD-Pancreas datasets. Segmentation performance was evaluated using DSC (%), and 95HD (mm). Evaluation results were reported as Mean \pm Std or Median [25% Q1,75% Q3]. All experiments were performed using 5-fold cross-validation with the same partition. The best and the second performances are highlighted by **bold** and underline. (*: $p < 0.01$ with Wilcoxon signed-rank test between DMC-Net and each method.)

Models	Methods	TCIA		MSD				Average Mean DSC
		Pancreas Mean DSC	Pancreas Mean 95HD	Pancreas Mean DSC	Pancreas Median 95HD	Tumor Mean DSC	Tumor Median 95HD	
2D	UNet	82.80 ± 7.05	6.14 ± 3.64	77.39 ± 9.46	5.80 [4.61,9.24]	36.72 ± 30.84	14.98 [6.22,50.05]	57.06
	DMRC-Net	84.08 ± 5.78	4.47 ± 3.62	<u>78.95</u> ± 9.24	<u>4.86</u> [3.56,6.34]	<u>39.81</u> ± 30.60	<u>10.66</u> [5.49,45.56]	<u>59.38</u>
	DMSC-Net	<u>84.39</u> ± 6.30	<u>4.43</u> ± 3.21	78.60 ± 9.03	5.00 [4.12,6.52]	38.28 ± 30.39	13.71 [5.37,39.66]	58.44
	DMC-Net	85.64* ± 3.93	3.80* ± 1.28	79.82* ± 8.32	4.63* [3.42,6.50]	42.07* ± 25.20	10.06* [4.44,28.27]	60.95*
3D	UNet	83.56 ± 6.43	5.06 ± 4.74	80.34 ± 8.37	4.63 [3.27,6.28]	52.31 ± 32.48	6.86 [3.38,19.88]	66.32
	DMRC-Net	<u>85.62</u> ± 4.62	3.69 ± 2.70	<u>81.44</u> ± 7.57	4.28 [3.29,5.32]	57.10 ± 31.09	<u>5.00</u> [3.2,12.83]	69.27
	DMSC-Net	85.67 ± 4.86	<u>3.74</u> ± 2.92	81.36 ± 7.47	<u>4.20</u> [3.11,5.43]	<u>57.37</u> ± 30.03	5.25 [3.24,11.33]	<u>69.36</u>
	DMC-Net	87.97* ± 3.52	2.83* ± 0.73	82.92* ± 6.91	4.08* [3.04,5.13]	60.71* ± 27.02	4.50* [2.86,10.71]	71.81*

On the MSD dataset, we only compared our 2D-DMC-Net with 2D nnU-Net Isensee et al. (2021), since few 2D segmentation methods were applied to this dataset. We also compared our 3D-DMC-Net with eight 3D methods, namely, V-Net Milletari et al. (2016), V-NAS Zhu et al. (2019), C2FNAS Yu et al. (2020), 3D nnU-Net Isensee et al. (2021), SAR Zhang et al. (2021b), Distill DSM Maheshwari et al. (2021), DiNTS He et al. (2021), and HyperSegNAS Peng et al. (2022). Table 2 presents the comparison results of these methods. Our 2D DMC-Net outperforms 2D nnU-Net on both pancreas and pancreatic tumor segmentation, thus achieving a superior performance in average segmentation from both two classes. Furthermore, when compared with other 3D methods, our 3D-DMC-Net demonstrated superior performance in both pancreas and pancreatic tumor segmentation. Specifically, it achieves the highest DSC in pancreas segmentation, pancreas tumor segmentation, and on average.

3.4. Ablation study on DMRC and DMSC modules

We conducted an ablation study on both 2D and 3D DMC-Net to evaluate the contributions of our DMRC and DMSC modules on improving pancreas segmentation accuracy. This ablation study was performed using both NIH TCIA-Pancreas and MSD Pancreas datasets.

We compared the segmentation performance between our DMC-Net and U-Net baselines. The U-Net was implemented following a similar design as DMC-Net in the number of layers and the number of feature maps in each layer. In this U-Net, each layer in both the encoder and decoder utilized a convolutional block consisting of two convolutional layers.

For 2D implementations, each convolutional layer had a 3×3 kernel, while for 3D implementations, each convolutional layer had a $3 \times 3 \times 3$ kernel. The 2D DMRC-Net was implemented using our 2D DMRC module to replace the first convolutional layer in each convolution block in all layers. The 2D DMSC-Net was built using our 2D DMSC module to replace the first convolutional layer in each convolution block in all layers. The same design was implemented to 3D DMSC-Net and 3D DMRC-Net.

Table 3 presents the results of our ablation study. Specifically, we observed that incorporating either the DMRC or DMSC modules into both 2D and 3D U-Net (DMRC-Net and DMSC-Net) resulted in superior segmentation performance than the U-Net, as measured by DSC and 95HD on the TCIA-Pancreas dataset. Additionally, the DMC-Net, incorporating both modules, consistently outperformed all other networks, demonstrating that the integration of our DMRC and DMSC modules may enhance the segmentation performance of U-Net. Subsequently, we conducted a similar ablation study on the MSD-Pancreas dataset. Integrating either the DMRC or DMSC modules into both 2D and 3D U-Net (DMRC-Net and DMSC-Net) enhanced the segmentation capabilities of U-Net for both pancreas and pancreatic tumors. Implementing DMC-Net by integrating modules achieved the highest segmentation accuracy in terms of DSC and 95HD. Figure 3 and Figure 4 further illustrate the effectiveness of our modules in improving pancreas segmentation on the TCIA-Pancreas and MSD-Pancreas datasets, respectively.

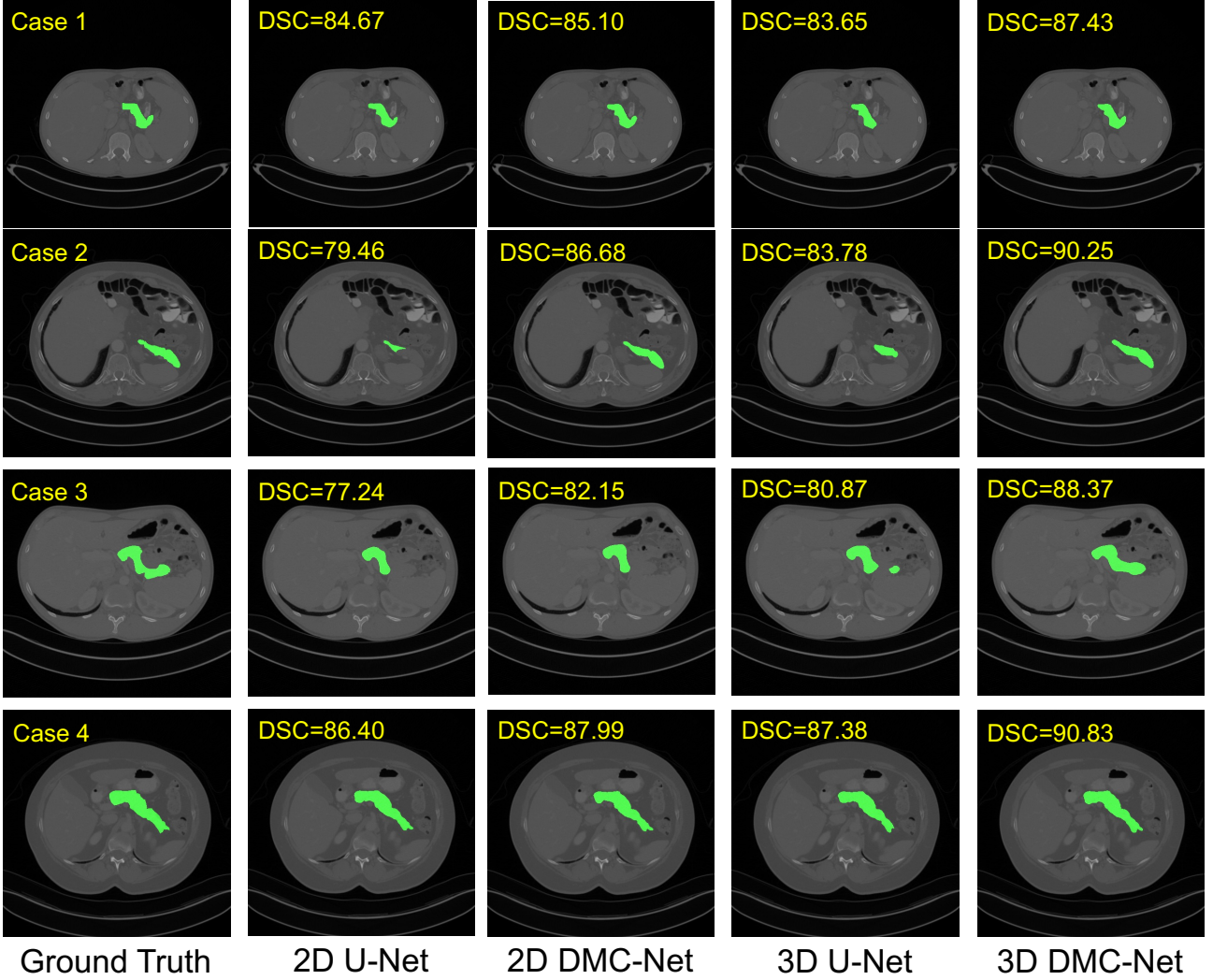


Figure 3: Visualizations of the pancreas segmentation results on the NIH TCIA-Pancreas dataset. The pancreas is marked in green. 2D DMC-Net shows better segmentation quality than 2D U-Net, and 3D DMC-Net shows better segmentation quality than 3D U-Net.

3.5. Ablation study on lightweight designs

Next, we conducted ablation studies to evaluate the importance of the lightweight design of DMRC and DMSC modules. First, we focused on assessing the importance of implementing the average pooling in 2D DMRC-Net using filters of size 4 and stride 4 (4×4 AvgPool) by comparing it with an implementation that uses filters of size 2 and stride 2 (2×2 AvgPool). Specifically, we evaluated the two architectures in terms of segmentation performance and computational complexity. Subsequently, we assessed the impact of the lightweight depthwise convolution in the 2D DMSC modules by comparing the segmentation performance and computational complexity of different DMSC-Nets. Specifically, we tested DMSC-Nets with 5×5 convolutional layers (5×5 Conv), 5×5 depth-wise convolutional layers (5×5 DWConv), 7×7 convolutional layers (7×7 Conv), and 7×7 depth-wise convolutional layers

(7×7 DWConv). The same ablation study was implemented for 3D DMRC and DMSC modules.

Table 4 presents the results of lightweight design analysis. The design of the 2D DMRC module showed that the DMRC-Net with 4×4 average pooling layers achieved better segmentation performance and lower computational complexity (higher DSC and 95HD values, and lower FLOPs). Similarly, using $4 \times 4 \times 4$ average pooling layers in the 3D DMRC module resulted in superior segmentation performance and lower computational complexity. Thus, this lightweight design was applied to both 2D and 3D DMRC modules.

We did not apply the lightweight design to our 2D DMSC module. Specifically, evaluating this lightweight design of DMSC modules showed that 2D DMSC-Net equipped with

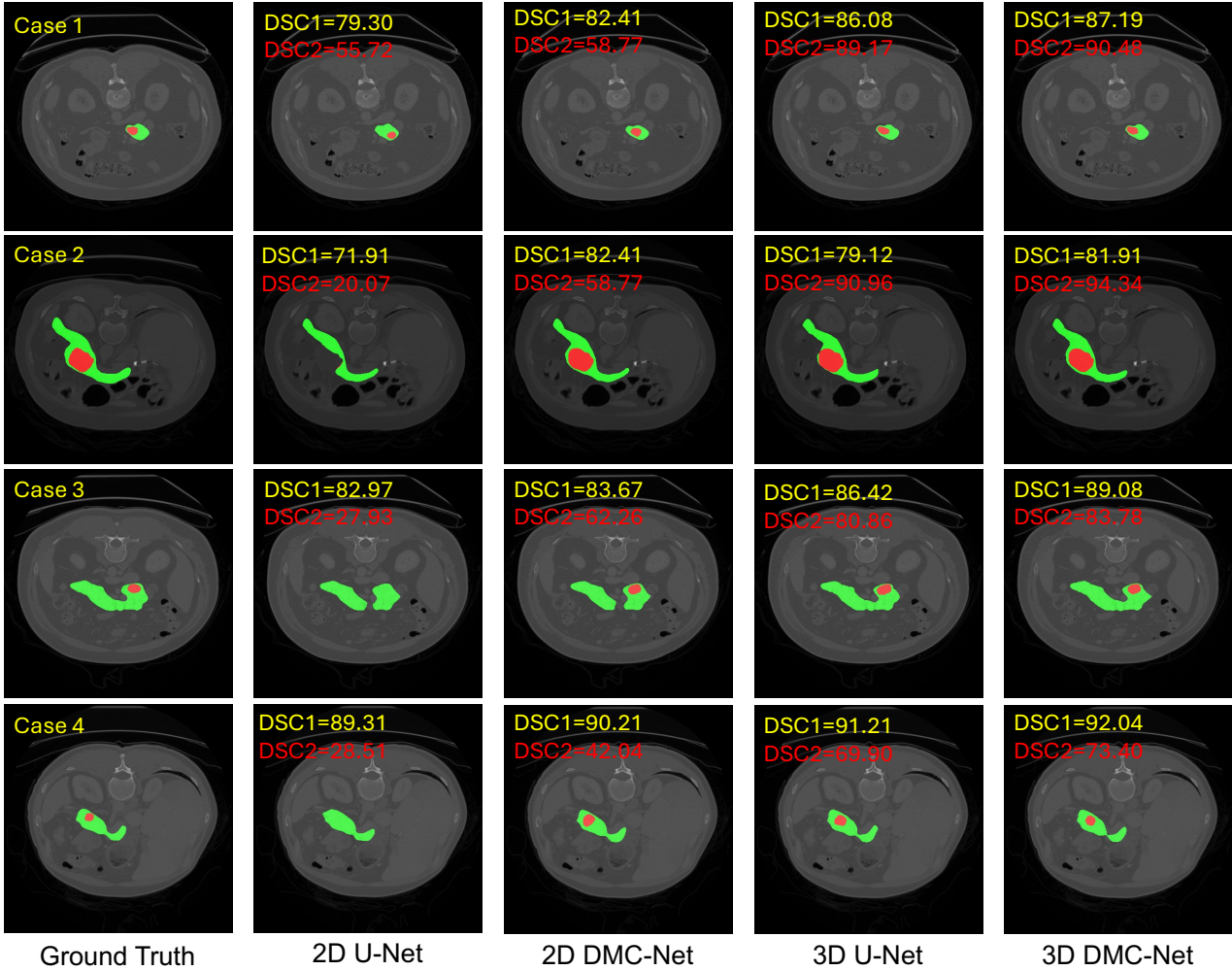


Figure 4: Visualizations of the pancreas and pancreatic mass segmentation results on the MSD-Pancreas dataset. The pancreas is marked in green, and the tumor is marked in red. 2D DMC-Net shows better segmentation quality than 2D U-Net, and 3D DMC-Net shows better segmentation quality than 3D U-Net.

5×5 convolutional layers achieved the best segmentation performance. On the contrary, 3D DMSC-Net with the lightweight design ($5 \times 5 \times 5$ DWConv) demonstrated the highest segmentation performance and the lowest computational complexity. Thus, we applied the lightweight design to 3D DMSC modules and used $5 \times 5 \times 5$ depth-wise convolutional layers instead of $5 \times 5 \times 5$ convolutional layers.

4. Conclusions

We proposed a Dynamic Multi-scale and Multi-resolution Convolution network (DMC-Net) for the automatic pancreas and pancreatic mass segmentation from CT images. This network employs novel Dynamic Multi-Scale Convolution (DMSC) and Dynamic Multi-Resolution Convolution (DMRC) modules, whose goal is to improve the representation capabilities of standard convolutional layers by capturing features and various scales and utilizing global contextual information. Our experimental analysis

demonstrated that the proposed modules may improve the segmentation performance of the network. An important component of the proposed architecture was the emphasis on adopting lightweight designs for the proposed convolutional layers. This facilitates the integration of the proposed modules into existing CNN architectures without requiring any changes in their macro-architectures. The experimental results showcased the superior performance of our 2D and 3D DMC-Net on two pancreas segmentation benchmarks compared to state-of-the-art methods. Lastly, we demonstrated that the use of the proposed DMSC and DMRC modules may improve the segmentation accuracy of CNNs without increasing the computational complexity compared to baseline CNN architectures.

Declaration of competing interests

The authors declare that they have no known competing financial interests or personal relationships that could have appeared to influence the work reported in this paper.

Table 4

The results of lightweight design analysis on the TCIA-Pancreas dataset. The segmentation performance was evaluated using DSC (%) and 95HD (mm). The computational complexity of the networks was evaluated using Params (M) and FLOPs (G). All experiments were implemented using 5-fold cross-validation with the same partition. The best segmentation performance and lower computational complexity in each method are highlighted by **bold**.

Models	Methods	Lightweight design	DSC	95HD	Params	FLOPs
2D	U-Net	-	82.80	6.14	22.80	94.86
	DMRC-Net	2 × 2 AvgPool	83.32	4.52	43.77	145.47
		4 × 4 AvgPool (ours)	84.08	4.47	43.77	138.86
	DMSC-Net	5 × 5 Conv (ours)	84.39	4.43	89.61	343.13
		5 × 5 DWConv	83.32	4.74	38.49	147.80
		7 × 7 Conv	83.26	4.72	139.89	536.81
	7 × 7 DWConv	83.18	4.81	38.61	150.15	
3D	U-Net	-	83.56	5.06	25.89	1398.81
	DMRC-Net	2 × 2 AvgPool	85.63	3.71	47.86	2098.93
		4 × 4 AvgPool (ours)	85.62	3.69	47.86	2011.70
	DMSC-Net	5 × 5 × 5 Conv	85.53	3.89	138.35	6766.37
		5 × 5 × 5 DWConv (ours)	85.67	3.74	41.02	2140.72
		7 × 7 × 7 Conv	85.55	3.76	309.35	15061.43
	7 × 7 × 7 DWConv	85.54	3.78	41.66	2337.84	

Acknowledgments

Computations were performed using the facilities of the Washington University Research Computing and Informatics Facility (RCIF). The RCIF has received funding from NIH S10 program grants: 1S10OD025200-01A1 and 1S10OD030477-01.

Funding

This work was supported by NIH grant U24 CA258483.

CRedit authorship contribution statement

JY: conceptualization, methodology, formal analysis, writing the original draft, reviewing, and editing, visualization; DM: methodology, writing, reviewing, and editing, supervision; AS: methodology, writing, reviewing, and editing, supervision.

References

- Antonelli, M., Reinke, A., Bakas, S., Farahani, K., Kopp-Schneider, A., Landman, B.A., Litjens, G., Menze, B., Ronneberger, O., Summers, R.M., et al., 2022. The medical segmentation decathlon. *Nature communications* 13, 4128.
- Aslani, S., Dayan, M., Storelli, L., Filippi, M., Murino, V., Rocca, M.A., Sona, D., 2019. Multi-branch convolutional neural network for multiple sclerosis lesion segmentation. *NeuroImage* 196, 1–15.
- Badrinarayanan, V., Kendall, A., Cipolla, R., 2017. Segnet: A deep convolutional encoder-decoder architecture for image segmentation. *IEEE transactions on pattern analysis and machine intelligence* 39, 2481–2495.
- Cai, J., Lu, L., Xie, Y., Xing, F., Yang, L., 2017. Improving deep pancreas segmentation in ct and mri images via recurrent neural contextual learning and direct loss function. *ArXiv abs/1707.04912*.
- Chen, G., Dai, Y., Zhang, J., Yin, X., Cui, L., 2022a. Mbanet: Multi-branch aware network for kidney ultrasound images segmentation. *Computers in biology and medicine* 141, 105140.
- Chen, H., Liu, Y., Shi, Z., Lyu, Y., 2022b. Pancreas segmentation by two-view feature learning and multi-scale supervision. *Biomedical Signal Processing and Control* 74, 103519.
- Chen, L.C., Barron, J.T., Papandreou, G., Murphy, K., Yuille, A.L., 2016. Semantic image segmentation with task-specific edge detection using cnns and a discriminatively trained domain transform, in: *Proceedings of the IEEE conference on computer vision and pattern recognition*, pp. 4545–4554.
- Chen, L.C., Papandreou, G., Kokkinos, I., Murphy, K., Yuille, A.L., 2017. Deeplab: Semantic image segmentation with deep convolutional nets, atrous convolution, and fully connected crfs. *IEEE transactions on pattern analysis and machine intelligence* 40, 834–848.
- Çiçek, Ö., Abdulkadir, A., Lienkamp, S.S., Brox, T., Ronneberger, O., 2016. 3d u-net: learning dense volumetric segmentation from sparse annotation, in: *International conference on medical image computing and computer-assisted intervention*, Springer. pp. 424–432.
- Ding, X., Zhang, X., Han, J., Ding, G., 2022. Scaling up your kernels to 31x31: Revisiting large kernel design in cnns, in: *Proceedings of the IEEE/CVF conference on computer vision and pattern recognition*, pp. 11963–11975.
- Fu, J., Liu, J., Tian, H., Li, Y., Bao, Y., Fang, Z., Lu, H., 2019. Dual attention network for scene segmentation, in: *Proceedings of the IEEE/CVF conference on computer vision and pattern recognition*, pp. 3146–3154.
- Guo, M.H., Lu, C.Z., Hou, Q., Liu, Z., Cheng, M.M., Hu, S.M., 2022. Segnext: Rethinking convolutional attention design for semantic segmentation. *Advances in Neural Information Processing Systems* 35, 1140–1156.
- Hariharan, B., Arbeláez, P., Girshick, R., Malik, J., 2014. Simultaneous detection and segmentation, in: *European conference on computer vision*, Springer. pp. 297–312.
- He, J., Deng, Z., Qiao, Y., 2019. Dynamic multi-scale filters for semantic segmentation, in: *Proceedings of the IEEE/CVF international conference on computer vision*, pp. 3562–3572.
- He, Y., Yang, D., Roth, H., Zhao, C., Xu, D., 2021. Dints: Differentiable neural network topology search for 3d medical image segmentation, in: *Proceedings of the IEEE/CVF conference on computer vision and pattern recognition*, pp. 5841–5850.

- Holger, R., Amal, F., Evrim, T., Le, L., Jiamin, L., Summers, R.M., 2016. Data from pancreas-ct, in: The Cancer Imaging Archive, <https://doi.org/10.7937/K9/TCIA.2016.tNB1kqBU>.
- Hu, J., Shen, L., Sun, G., 2018. Squeeze-and-excitation networks, in: Proceedings of the IEEE conference on computer vision and pattern recognition, pp. 7132–7141.
- Hu, P., Li, X., Tian, Y., Tang, T., Zhou, T., Bai, X., Zhu, S., Liang, T., Li, J., 2020. Automatic pancreas segmentation in ct images with distance-based saliency-aware denseaspp network. *IEEE journal of biomedical and health informatics* 25, 1601–1611.
- Ibragimov, B., Xing, L., 2017. Segmentation of organs-at-risks in head and neck ct images using convolutional neural networks. *Medical physics* 44, 547–557.
- Isensee, F., Jaeger, P.F., Kohl, S.A., Petersen, J., Maier-Hein, K.H., 2021. nnu-net: a self-configuring method for deep learning-based biomedical image segmentation. *Nature methods* 18, 203–211.
- Kumar, H., DeSouza, S.V., Petrov, M.S., 2019. Automated pancreas segmentation from computed tomography and magnetic resonance images: A systematic review. *Computer methods and programs in biomedicine* 178, 319–328.
- Lee, H.H., Bao, S., Huo, Y., Landman, B.A., 2022. 3d ux-net: A large kernel volumetric convnet modernizing hierarchical transformer for medical image segmentation. *arXiv preprint arXiv:2209.15076*.
- Li, J., Liao, G., Sun, W., Sun, J., Sheng, T., Zhu, K., von Deneen, K.M., Zhang, Y., 2022. A 2.5 d semantic segmentation of the pancreas using attention guided dual context embedded u-net. *Neurocomputing* 480, 14–26.
- Lin, T.Y., Dollár, P., Girshick, R., He, K., Hariharan, B., Belongie, S., 2017. Feature pyramid networks for object detection, in: Proceedings of the IEEE conference on computer vision and pattern recognition, pp. 2117–2125.
- Liu, Z., Mao, H., Wu, C.Y., Feichtenhofer, C., Darrell, T., Xie, S., 2022. A convnet for the 2020s, in: Proceedings of the IEEE/CVF conference on computer vision and pattern recognition, pp. 11976–11986.
- Maheshwari, H., Goel, V., Sethuraman, R., Sheet, D., 2021. Distill dsm: Computationally efficient method for segmentation of medical imaging volumes, in: *Medical Imaging with Deep Learning*, PMLR. pp. 473–483.
- McGuigan, A., Kelly, P., Turkington, R.C., Jones, C., Coleman, H.G., McCain, R.S., 2018. Pancreatic cancer: A review of clinical diagnosis, epidemiology, treatment and outcomes. *World journal of gastroenterology* 24, 4846.
- Milletari, F., Navab, N., Ahmadi, S.A., 2016. V-net: Fully convolutional neural networks for volumetric medical image segmentation, in: 2016 fourth international conference on 3D vision (3DV), IEEE. pp. 565–571.
- Narin, A., Kaya, C., Pamuk, Z., 2021. Automatic detection of coronavirus disease (covid-19) using x-ray images and deep convolutional neural networks. *Pattern Analysis and Applications* 24, 1207–1220.
- Noh, H., Hong, S., Han, B., 2015. Learning deconvolution network for semantic segmentation, in: Proceedings of the IEEE international conference on computer vision, pp. 1520–1528.
- Peng, C., Myronenko, A., Hatamizadeh, A., Nath, V., Siddiquee, M.M.R., He, Y., Xu, D., Chellappa, R., Yang, D., 2022. Hypersegnas: Bridging one-shot neural architecture search with 3d medical image segmentation using hypernet, in: Proceedings of the IEEE/CVF Conference on Computer Vision and Pattern Recognition, pp. 20741–20751.
- Qiu, C., Liu, Z., Song, Y., Yin, J., Han, K., Zhu, Y., Liu, Y., Sheng, V.S., 2023. Rtunet: Residual transformer unet specifically for pancreas segmentation. *Biomedical Signal Processing and Control* 79, 104173.
- Ronneberger, O., Fischer, P., Brox, T., 2015. U-net: Convolutional networks for biomedical image segmentation, in: Navab, N., Hornegger, J., Wells, W.M., Frangi, A.F. (Eds.), *Medical Image Computing and Computer-Assisted Intervention – MICCAI 2015*, Springer International Publishing, Cham. pp. 234–241.
- Roth, H., Lu, L., Farag, A., Shin, H.C., Liu, J., Turkbey, B., Summers, R., 2015. Deeporgan: Multi-level deep convolutional networks for automated pancreas segmentation. doi:10.1007/978-3-319-24553-9_68.
- Roth, H., Lu, L., Lay, N., Harrison, A., Farag, A., Sohn, A., Summers, R., 2017. Spatial aggregation of holistically-nested convolutional neural networks for automated pancreas localization and segmentation. *Medical Image Analysis* 45. doi:10.1016/j.media.2018.01.006.
- Roth, H.R., Lu, L., Lay, N., Harrison, A.P., Farag, A., Sohn, A., Summers, R.M., 2018. Spatial aggregation of holistically-nested convolutional neural networks for automated pancreas localization and segmentation. *Medical image analysis* 45, 94–107.
- Schlemper, J., Oktay, O., Schaap, M., Heinrich, M., Kainz, B., Glocker, B., Rueckert, D., 2019. Attention gated networks: Learning to leverage salient regions in medical images. *Medical Image Analysis* 53, 197–207. URL: <https://www.sciencedirect.com/science/article/pii/S1361841518306133>, doi:<https://doi.org/10.1016/j.media.2019.01.012>.
- Seferbekov, S., Iglovikov, V., Buslaev, A., Shvets, A., 2018. Feature pyramid network for multi-class land segmentation, in: Proceedings of the IEEE conference on computer vision and pattern recognition workshops, pp. 272–275.
- Wang, C., Zhao, L., Liang, S., Zhang, L., Jia, J., Wei, Y., 2015. Object proposal by multi-branch hierarchical segmentation, in: Proceedings of the IEEE conference on computer vision and pattern recognition, pp. 3873–3881.
- Woo, S., Park, J., Lee, J.Y., Kweon, I.S., 2018. Cbam: Convolutional block attention module, in: Proceedings of the European conference on computer vision (ECCV), pp. 3–19.
- Yang, J., Marcus, D.S., Sotiras, A., 2023. Abdominal ct pancreas segmentation using multi-scale convolution with aggregated transformations, in: *Medical Imaging 2023: Computer-Aided Diagnosis*, SPIE. pp. 418–426.
- Yang, J., Qiu, P., Zhang, Y., Marcus, D.S., Sotiras, A., 2024. D-net: Dynamic large kernel with dynamic feature fusion for volumetric medical image segmentation. *arXiv preprint arXiv:2403.10674*.
- Yu, Q., Xie, L., Wang, Y., Zhou, Y., Fishman, E.K., Yuille, A.L., 2018. Recurrent saliency transformation network: Incorporating multi-stage visual cues for small organ segmentation, in: Proceedings of the IEEE conference on computer vision and pattern recognition, pp. 8280–8289.
- Yu, Q., Yang, D., Roth, H., Bai, Y., Zhang, Y., Yuille, A.L., Xu, D., 2020. C2fnas: Coarse-to-fine neural architecture search for 3d medical image segmentation, in: Proceedings of the IEEE/CVF Conference on Computer Vision and Pattern Recognition, pp. 4126–4135.
- Zhang, D., Zhang, J., Zhang, Q., Han, J., Zhang, S., Han, J., 2021a. Automatic pancreas segmentation based on lightweight dcnn modules and spatial prior propagation. *Pattern Recognition* 114, 107762.
- Zhang, X., Feng, S., Zhou, Y., Zhang, Y., Wang, Y., 2021b. Sar: Scale-aware restoration learning for 3d tumor segmentation, in: *Medical Image Computing and Computer Assisted Intervention–MICCAI 2021: 24th International Conference, Strasbourg, France, September 27–October 1, 2021, Proceedings, Part II* 24, Springer. pp. 124–133.
- Zhang, Y., Wu, J., Liu, Y., Chen, Y., Chen, W., Wu, E.X., Li, C., Tang, X., 2021c. A deep learning framework for pancreas segmentation with multi-atlas registration and 3d level-set. *Medical Image Analysis* 68, 101884.
- Zhao, N., Tong, N., Ruan, D., Sheng, K., 2019a. Fully automated pancreas segmentation with two-stage 3d convolutional neural networks, in: *International Conference on Medical Image Computing and Computer-Assisted Intervention*, Springer. pp. 201–209.
- Zhao, Q., Sheng, T., Wang, Y., Tang, Z., Chen, Y., Cai, L., Ling, H., 2019b. M2det: A single-shot object detector based on multi-level feature pyramid network, in: Proceedings of the AAAI conference on artificial intelligence, pp. 9259–9266.
- Zhao, X., Li, L., Lu, W., Tan, S., 2018. Tumor co-segmentation in pet/ct using multi-modality fully convolutional neural network. *Physics in Medicine & Biology* 64, 015011.
- Zheng, Y., Luo, J., 2023. Extension–contraction transformation network for pancreas segmentation in abdominal ct scans. *Computers in Biology and Medicine* 152, 106410.
- Zhong, Z., Lin, Z.Q., Bidart, R., Hu, X., Daya, I.B., Li, Z., Zheng, W.S., Li, J., Wong, A., 2020. Squeeze-and-attention networks for semantic segmentation, in: Proceedings of the IEEE/CVF conference on computer vision and pattern recognition, pp. 13065–13074.

- Zhou, Y., Xie, L., Shen, W., Wang, Y., Fishman, E., Yuille, A., 2017. A fixed-point model for pancreas segmentation in abdominal ct scans, pp. 693–701. doi:10.1007/978-3-319-66182-7_79.
- Zhou, Z., Rahman Siddiquee, M.M., Tajbakhsh, N., Liang, J., 2018. Unet++: A nested u-net architecture for medical image segmentation, in: Deep learning in medical image analysis and multimodal learning for clinical decision support. Springer, pp. 3–11.
- Zhu, Z., Liu, C., Yang, D., Yuille, A., Xu, D., 2019. V-nas: Neural architecture search for volumetric medical image segmentation, in: 2019 International conference on 3d vision (3DV), IEEE. pp. 240–248.